Decomposing the Oxygen Signal in the Ocean Interior: Beyond Decomposing Organic Matter

Nicolas Cassar, David Nicholson, Samar Khatiwala, Ellen Cliff

AGU
ADVANCING EARTH AND SPACE SCIENCE

Geophysical Research Letters®

Key Points:

- We propose the new tracer $[O_2]_{bio}$, estimated based on the dissolved O_2/Ar ratio, to estimate oxygen utilization at depth
- We assess the value in $[O_2]_{bio}$ as a proxy for oxygen utilization in the ocean interior and gas exchange at sites of deepwater formation
- When physical processes dominate O_2 disequilibrium at the regions of deepwater formation, the new tracer performs better than apparent oxygen utilization (AOU)

Decomposing the Oxygen Signal in the Ocean Interior: Beyond Decomposing Organic Matter

Nicolas Cassar[1,2] , **David Nicholson[3]** , **Samar Khatiwala[4]** , and **Ellen Cliff[4]**

[1]Division of Earth and Climate Sciences, Nicholas School of the Environment, Duke University, Durham, NC, USA, [2]CNRS, Université de Brest, IRD, Ifremer, LEMAR, Plouzané, France, [3]Department of Marine Chemistry and Geochemistry, Woods Hole Oceanographic Institution, Woods Hole, MA, USA, [4]Department of Earth Sciences, University of Oxford, Oxford, UK

Abstract In the subsurface ocean, O_2 depleted because of organic matter remineralization is generally estimated based on apparent oxygen utilization (AOU). However, AOU is an imperfect measure of oxygen utilization because of O_2 air-sea disequilibrium at the site of deepwater formation. Recent methodological and instrumental advances have paved the way to further deconvolve the processes driving the O_2 signature. Using numerical model simulations of the global ocean, we show that the measurements of the dissolved O_2/Ar ratio, which so far have been confined to the ocean surface, can provide improved estimates of oxygen utilization, especially in regions where the disequilibrium at the site of deepwater formation is associated with physical processes. We discuss applications of this new approach and implications for the current tracers relying on O_2 such as remineralization ratios, respiratory quotients, and preformed nutrients. Finally, we propose a new composite geochemical tracer, $[O_2]_{bio}^*$ combining dissolved O_2/Ar and phosphate concentration. Being insensitive to photosynthesis and respiration, the change in this new tracer reflects gas exchange at the air-sea interface at the sites of deepwater formation.

Plain Language Summary Oxygen utilization in the ocean interior offers an insight into organic matter remineralization and the strength of the biological carbon pump. However, the oxygen concentration in the ocean interior is also impacted by additional biotic and abiotic processes occurring at the sites of deepwater formation and during transit in the ocean interior. In this study, we summarize, formalize, and model these processes to explore how decomposing the O_2 signal at depth with new tools can provide a new insight and more refined budgets of the broad-scale oceanic biogeochemical cycling of oxygen and nutrients. This is particularly important in light of the recent evidence that the role of physical processes in the regions of convective deepwater formation may currently be underestimated.

1. Introduction

The ocean biological pump is a critical component of the Earth's climate system, serving as a vector for the transfer of carbon from the atmosphere to the deep ocean. At depth, the remineralization of organic matter leads to Redfieldian-like stoichiometry in oxygen, carbon, and various nutrients. Deviations from this predictable elemental stoichiometry have provided valuable insight into sources and sinks of nutrients. For example, small anomalies from the elemental stoichiometric relation between phosphate (PO_4) and nitrate (NO_3) inform us about the magnitude and variability of nitrogen fixation and denitrification (Deutsch et al., 2001; Gruber & Sarmiento, 1997). While the correlation of NO_3 with PO_4 at depth is strong, the same cannot be said for oxygen (O_2) versus PO_4 (Figure S1). This is in part attributable to varying O_2/PO_4 stoichiometry, preformed PO_4, and physical processes obscuring the Redfieldian behavior of O_2. A significant source of decoupling occurs at the ocean surface, where ventilation in part or fully resets the O_2 through the exchange with the atmosphere, thereby decoupling O_2 and PO_4. In this study, we decompose the O_2 signal into biotic and abiotic preformed and transit components to explore the processes driving O_2 variability in the ocean interior (Figure 1). We combine them with simulations of dissolved argon (Ar) to propose the measurement of dissolved O_2/Ar ratio at depth to improve estimates of the true oxygen utilization and remineralization ratios in the ocean interior.
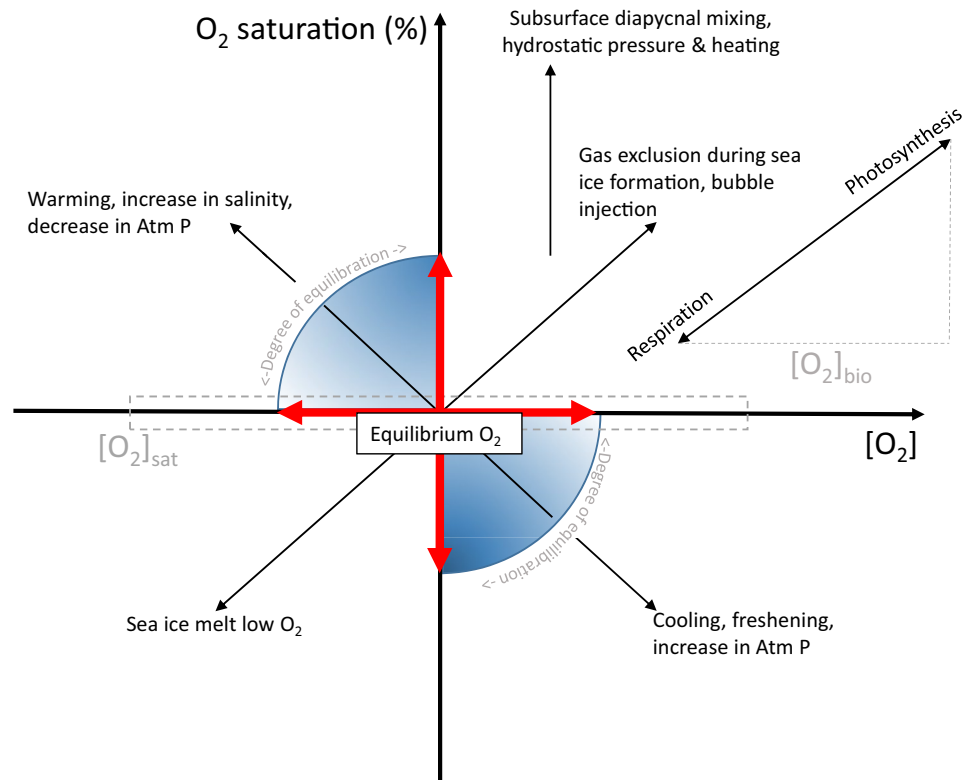
Figure 1. Biotic and abiotic processes influencing dissolved oxygen saturation and concentration in the ocean. Air-sea gas exchange (not shown) tends to bring O_2 back to equilibration with the atmosphere (origin on the plot). $[O_2]_{sat}$, as defined in our study, is the O_2 concentration at equilibrium. The degree to which changes in atmospheric pressure, seawater salinity, and temperature influence the saturation and equilibrium concentration depends on the extent of equilibration with the atmosphere. For example, a decrease in temperature with full equilibration leads to an increase in oxygen concentration at saturation $[O_2]_{sat}$. Conversely, the same change in temperature with no gas exchange (e.g., subsurface) will lead to an O_2 undersaturation anomaly with no change in $[O_2]$ (i.e., decrease in $[O_2]_{phy}$ is compensated by an increase in $[O_2]_{sat}$). Subsurface processes, including the mixing of water masses with differing temperature and salinity (including diapycnal mixing), hydrostatic pressure, and heating, change the O_2 saturation but not the total O_2 concentration. However, they change the relative contribution of $[O_2]_{sat}$ and $[O_2]_{phy}$ to $[O_2]$. For example, a reduction in $[O_2]_{sat}$ associated with subsurface heating or diapycnal mixing (lower O_2 solubility) is perfectly balanced by an increase in $[O_2]_{phy}$ with no net impact on $[O_2]$. The impact of diapycnal mixing on the gas saturation is greatest in the thermocline where temperature gradients are steepest. $[O_2]_{bio}$, as defined in our study, is the horizontal vector associated with photosynthesis and respiration/remineralization. $[O_2]_{phy}$, not shown in this figure, is equal to the saturation anomaly (ordinate) associated with the physical processes times the concentration at saturation. The effect of glacial melt is also not shown for clarity. While subsurface glacial melt increases $[O_2]$ because of the high concentration in glacial ice relative to seawater (Hellmer et al., 1985; Jenkins, 1999; Martinerie et al., 1992), its impact on saturation ($[O_2]_{phy}$) can be positive or negative depending, among other things, on the effective potential temperature of the ice.

2. Biological and Physical Preformed and Transit O_2

The biological pump transfers (or "pumps") inorganic carbon against a concentration gradient from the ocean surface to the deep ocean, akin to the photosynthetic transfer of protons against a concentration gradient into the thylakoid lumen generating a proton motive force. Both pumps are driven by light energy, and both have oxygen as an ultimate by-product. In fact, oxygen utilization at depth is thought to be a reliable metric of the strength of the biological carbon pump (Koeve et al., 2020), with depth profiles of O_2 almost mirroring dissolved inorganic carbon (DIC) (Figure S2). Deviations from this mirror image result from various processes and the differing equilibration timescales decoupling the DIC and O_2 properties. The dissolved O_2 concentration in the ocean ($[O_2]$; brackets hereafter refer to concentrations) can be decomposed as follows:

$$[O_2] = [O_2]_{sat} + [O_2]_{phy} + [O_2]_{bio} \tag{1}$$

where $[O_2]_{sat}$ is the saturation O_2 concentration calculated using the in situ temperature and salinity, and $[O_2]_{bio}$ and $[O_2]_{phy}$ reflect the deviations in O_2 concentration from saturation associated with biological and physical processes, respectively. $[O_2]_{bio}$ is conservative with respect to physical processes, although the physical processes can redistribute it. As we will show below, the dissolved O_2/Ar ratio can be used as a proxy for $[O_2]_{bio}$. Note that in Cassar et al. (2011), the $[O_2]_{phy}$ nomenclature refers to ($[O_2]_{sat} + [O_2]_{phy}$). Here, it refers to the concentration associated with the anomaly (i.e., supersaturation instead of saturation). We use the terms physical and abiotic interchangeably. Abiotic refers to nonliving chemical and physical processes, which in our discussion revolve around physical chemistry. When occurring on timescales faster than air-sea gas exchange, physical (e.g., bubble injection and temperature change) and biological (photosynthesis and respiration, including remineralization) processes lead O_2 to deviate from saturation. Redfield et al. (1963) described the nutrient pool as the sum of remineralized and preformed fractions. Similarly, the oxygen measured at the depth is a function of a preformed signature and processes occurring in transit. We further decompose the biological and physical signals into preformed (*pre*) and transit (where Δ refers to the transit change) components:

$$[O_2] = [O_2]_{sat} + [O_2]_{phy\,pre} + \Delta[O_2]_{phy} + [O_2]_{bio\,pre} + \Delta[O_2]_{rem} \tag{2}$$

The subscript "*rem*" refers to the remineralization. This decomposition is similar to the recent study by Cliff et al. (2021), although what is referred to as "$O_{2,\,eq}$" in that study is further decomposed here into $\left([O_2]_{sat} + \Delta[O_2]_{phy}\right)$. While hydrostatic pressure, subsurface heating, and mixing of water masses with differing temperature and salinity (including diapycnal mixing) affect saturation (Emerson et al., 2012; Enns et al., 1965; Henning et al., 2006; Ito & Deutsch, 2006; Ito et al., 2007; Klots, 1961), physical processes will not impact the total O_2 concentration $\left([O_2]\right)$, which is conservative below the surface for inert gases (Hamme & Emerson, 2002). However, such processes will impact the relative contribution of $[O_2]_{sat}$ and $\Delta[O_2]_{phy}$ to $[O_2]$. For example, the lower O_2 solubility (i.e., decrease in $[O_2]_{sat}$) associated with subsurface heating and diapycnal mixing is compensated by an increase in O_2 supersaturation anomaly (increase in $\Delta[O_2]_{phy}$), resulting in no change in $[O_2]$ (Figure 2).

The true oxygen utilization (TOU) is defined as the biological oxygen demand of waters after isolation from the atmosphere:

$$-\text{TOU} = \Delta[O_2]_{Rem} = [O_2]_{bio} - [O_2]_{bio\,pre} = [O_2] - \left([O_2]_{sat} + [O_2]_{phy\,pre} + \Delta[O_2]_{phy} + [O_2]_{bio\,pre}\right) \tag{3}$$

AOU, calculated as $\left([O_2]_{sat} - [O_2]\right)$, is an approximation of TOU under the assumption that $\left([O_2]_{phy\,pre} + \Delta[O_2]_{phy} + [O_2]_{bio\,pre}\right) = 0$ in Equation 3. In reality, AOU generally overestimates TOU because of oxygen undersaturation at the sites of deepwater formation (Broecker et al., 1991; Cliff et al., 2021; Duteil et al., 2013; Ito et al., 2004; Khatiwala et al., 2019; Redfield et al., 1963; Shiller, 1981). The undersaturation results from physical processes such as heat fluxes, impairment of gas exchange by sea ice (Hamme & Severinghaus, 2007), and entrainment of underlying waters with a biological O_2 undersaturation (i.e., $[O_2]_{phy\,pre} + [O_2]_{bio\,pre} < 0$). This disequilibrium is difficult to measure because the ventilation regions are inhospitable in winter when deep waters are formed. However, floats have provided glimpses of large O_2 undersaturations (Kortzinger et al., 2004; Wolf et al., 2018). Using a global ocean circulation-biogeochemical model with explicit TOU, Ito et al. (2004) showed that the AOU bias associated with surface O_2 disequilibrium at high latitudes can be significant. Cliff et al. (2021) also used a model to explicitly simulate TOU but furthermore decomposed the disequilibrium O_2 into physically and biologically mediated components (here called $[O_2]_{phy\,pre}$ and $[O_2]_{bio\,pre}$, respectively). In their data-constrained model, ~11% of the reduction in the ocean's inventory of O_2 from its equilibrium value is due to biological disequilibrium, whereas ~3% is from physical disequilibrium. Duteil et al. (2013) proposed to improve on TOU estimates by approximating the preformed oxygen concentration with the mean oxygen disequilibrium below the seasonal mixed layer at 100-m water depth at the sites of deepwater formation. A potential issue with such an approach is that $[O_2]$ in the ocean interior reflects a poorly characterized amalgam of many surface regions (DeVries & Primeau, 2011; Haine & Hall, 2002; Khatiwala et al., 2012; Primeau, 2005).
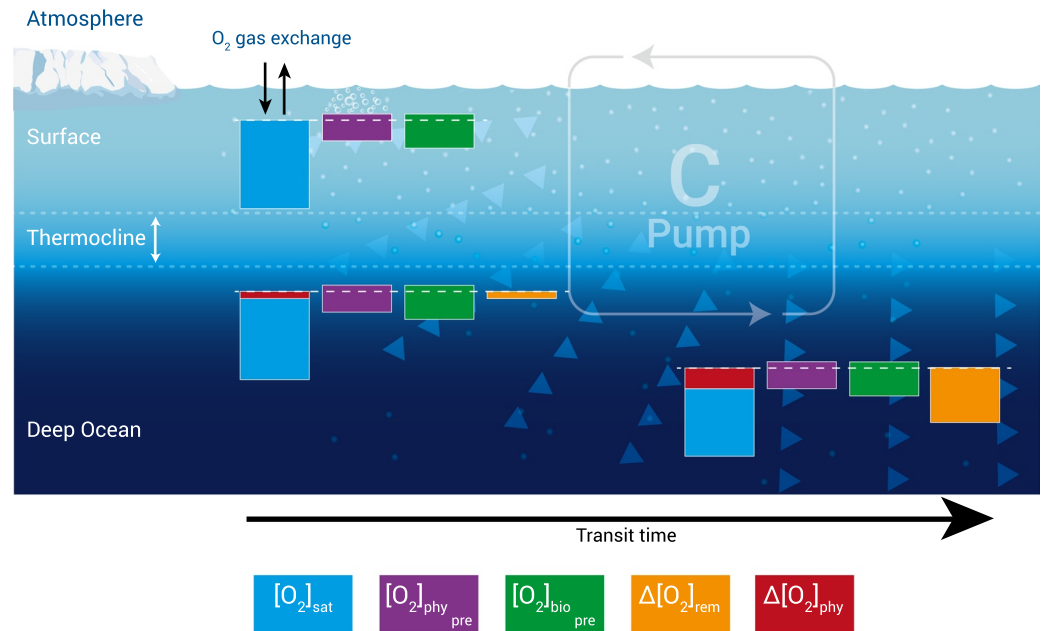
Figure 2. Conceptual diagram representing the physical and biological processes influencing preformed and transit oxygen concentration. Physical processes, such as bubble injection, changes in atmospheric pressure, mixing of water masses, and changes in temperature, lead to a preformed physical O_2 concentration. Ventilation of O_2-depleted waters associated with remineralization at depth and respiration and photosynthesis at the ocean surface lead to a preformed biological O_2 concentration. All these physical and biological processes must occur on timescales faster than the equilibration in order for the preformed concentrations to deviate from zero. Equilibration erases the preformed signals. Factors such as ice cover, mixed-layer depth, and wind speed impact the residence time and equilibration time of O_2. The O_2 concentration measured at depth is a function of these preformed signals and physical processes and remineralization during transit. Phosphate behaves similarly without the influence of physical processes and exchange with the atmosphere.

3. Estimating $[O_2]_{bio}$ With the Dissolved Elemental O_2/Ar Ratio

By design, $[O_2]_{bio}$ is conservative with respect to the physical processes. Based on Equation 3, TOU can be accurately estimated from $[O_2]_{bio}$ if the preformed biological signal is nil or well known and can be approximated in regions where physical processes dominate the O_2 disequilibrium (i.e., $[O_2]_{phy} \gg [O_2]_{biopre}$).

We propose that $[O_2]_{bio}$ can be estimated from the dissolved elemental ratio O_2 and argon (Ar). O_2 and Ar have similar solubility and diffusivity properties (Figure S3) but the latter is biologically inert (Garcia & Gordon, 1992; Wise & Houghton, 1966). An equation analogous to Equation 1 can be written for Ar:

$$\left[Ar \right] = \left(\left[Ar \right]_{sat} + \left[Ar \right]_{phy} \right) \tag{4}$$

and from Equations 1 and 4:

$$\frac{\left(\left[O_2 \right]_{sat} + \left[O_2 \right]_{phy} \right)}{\left[O_2 \right]_{sat}} \approx \frac{\left(\left[Ar \right]_{sat} + \left[Ar \right]_{phy} \right)}{\left[Ar \right]_{sat}} = \frac{\left[Ar \right]}{\left[Ar \right]_{sat}} \tag{5}$$

The two gases can be combined into a synthetic tracer of biological activity, which is conservative with respect to physical processes (Craig & Hayward, 1987). As shown in Cassar et al. (2011), $[O_2]_{bio}$ can therefore be estimated by combining Equations 1 and 5 (see supplement for full derivation):

$$\left[O_2 \right]_{bio} \approx \left[O_2 \right] - \frac{\left[Ar \right]}{\left[Ar \right]_{sat}} \left[O_2 \right]_{sat} = \frac{\left[Ar \right]}{\left[Ar \right]_{sat}} \left[O_2 \right]_{sat} \Delta \left(O_2/Ar \right) \tag{6}$$

where $\Delta\left(O_2/Ar\right) = \left[\left(O_2/Ar\right)/\left(O_2/Ar\right)_{\text{sat}} - 1\right]$. The approach has thus far exclusively been used at the ocean surface to estimate biological oxygen fluxes and net community production (Cassar et al., 2009, 2011; Gueguen & Tortell, 2008; Hamme et al., 2012; Huang et al., 2012; Long et al., 2011; Palevsky et al., 2013; Reuer et al., 2007; Spitzer & Jenkins, 1989). $[Ar]/[Ar]_{\text{sat}}$ on the very right-hand side of Equation 6 is generally assumed at saturation, but can be measured (Hamme & Emerson, 2002) or estimated from concurrent measurements of $\Delta\left(O_2/Ar\right)$ (by mass spectrometry, in situ or otherwise) and $[O_2]$ (Eveleth et al., 2014, 2017). Assuming that Ar is at saturation introduces a small error of <3% under most oceanic conditions away from waters influenced by ice dynamics (see also Figure S4). Similarly, the dissolved $[O_2]_{\text{phy}}$ can be estimated in the ocean interior through:

$$\left[O_2\right]_{\text{phy}} \approx \frac{\left[O_2\right]}{\left(1 + \Delta\left(O_2/Ar\right)\right)} - \left[O_2\right]_{\text{sat}} \tag{7}$$

The combination of O_2 and $\Delta\left(O_2/Ar\right)$ observations provides insight into the argon saturation anomaly at depth and $[O_2]_{\text{phy}}$, which reflects a varying contribution of physical processes at the site of ventilation and during transit at depth (Hamme et al., 2019; Ito & Deutsch, 2006).

4. The Added Value of Estimating TOU With $[O_2]_{\text{bio}}$

We now assess the added value of a TOU proxy based on the O_2/Ar estimates of $[O_2]_{\text{bio}}$. We combine the O_2 simulations of Cliff et al. (2021) in which TOU is modeled explicitly, with new argon simulations performed using an "offline" model (Khatiwala, 2007, 2018; Nicholson et al., 2016) driven by the same circulation and physical forcing fields, to compare the estimates derived from the approximations of AOU and $[O_2]_{\text{bio}}$. Our study can thus be viewed as an Ocean Observing System Simulation Experiment (OSSE). See the supplement for a description of the model.

We note that neither the O_2 nor Ar simulations account for some potentially important physical processes, including spatial variations in the atmospheric pressure and bubbles and gas exclusion during sea ice formation. The gas exclusion during the ice formation combined with brine rejection leads to large O_2 gas supersaturation (Top et al., 1985, 1988). During the winter (and during deepwater formation), the main effect will be a substantial increase in $[O_2]_{\text{phypre}}$, in opposition to the rapid cooling effect. In addition, recent observation and modeling efforts show that bubble-mediated fluxes may currently be substantially underestimated in regions of convective deepwater formation (Atamanchuk et al., 2020; Sun et al., 2017). Our OSSE simulations, which do not account for these processes, therefore could represent a conservative measure of the improvement of $[O_2]_{\text{bio}}$ estimates of TOU compared to AOU.

While AOU neglects $\left([O_2]_{\text{phy}} + [O_2]_{\text{biopre}}\right)$, a TOU estimate based on $[O_2]_{\text{bio}}$ removes one source of error $[O_2]_{\text{phy}}$ and the bias is due to $[O_2]_{\text{biopre}}$ alone. Figure 3 shows their relative performance (Figure 3a) and property-property plots of the factors influencing their performance (Figures 3b–3d). As expected, both AOU and $[O_2]_{\text{bio}}$ overestimate the TOU. The median overestimation with $[O_2]_{\text{bio}}$ is around 10%–15% lower than with AOU for the individual observations (Figure 3a), and around 5% for the ocean inventory (Figure S5) because it accounts for $[O_2]_{\text{biopre}}$ (RMSE of AOU and $[O_2]_{\text{bio}}$ relative to TOU are 40.5 and 34.8 mmol m^{-3}, respectively). The improvement is small because $[O_2]_{\text{biopre}}$ is generally larger than $[O_2]_{\text{phypre}}$ in these simulations (Figure S5). However, this is likely an underestimate because, as described above, potentially important processes have been neglected, and the improvement is substantially greater in some regions (as shown below). We note that including these other physical processes would also impact $[O_2]_{\text{biopre}}$. For example, bubbles facilitate air-sea gas removal of the $[O_2]_{\text{bio}}$ signal. Ice melt results in a conservative mixing of the sympagic and water-column $[O_2]_{\text{bio}}$ concentrations. According to the model's simulations, 20 (10)% of TOU estimates could be improved by more than 20 (50)% using $[O_2]_{\text{bio}}$ instead of AOU, as shown by a cumulative frequency distribution (Figure S6). As is evident in Figure 3b and from $-[O_2]_{\text{bio}}$ / TOU $=1 - [O_2]_{\text{biopre}}$ / TOU, the predictive power of $[O_2]_{\text{bio}}$ increases as $[O_2]_{\text{biopre}}$ / TOU decreases. In regions where $[O_2]_{\text{biopre}}$ is large, improvements in $[O_2]_{\text{bio}}$-based estimates of TOU will require better constraints on $[O_2]_{\text{biopre}}$. Conversely and as shown in Figure 3c, AOU's estimates of TOU improve as the preformed $[O_2]$ and $\Delta[O_2]_{\text{phy}}$
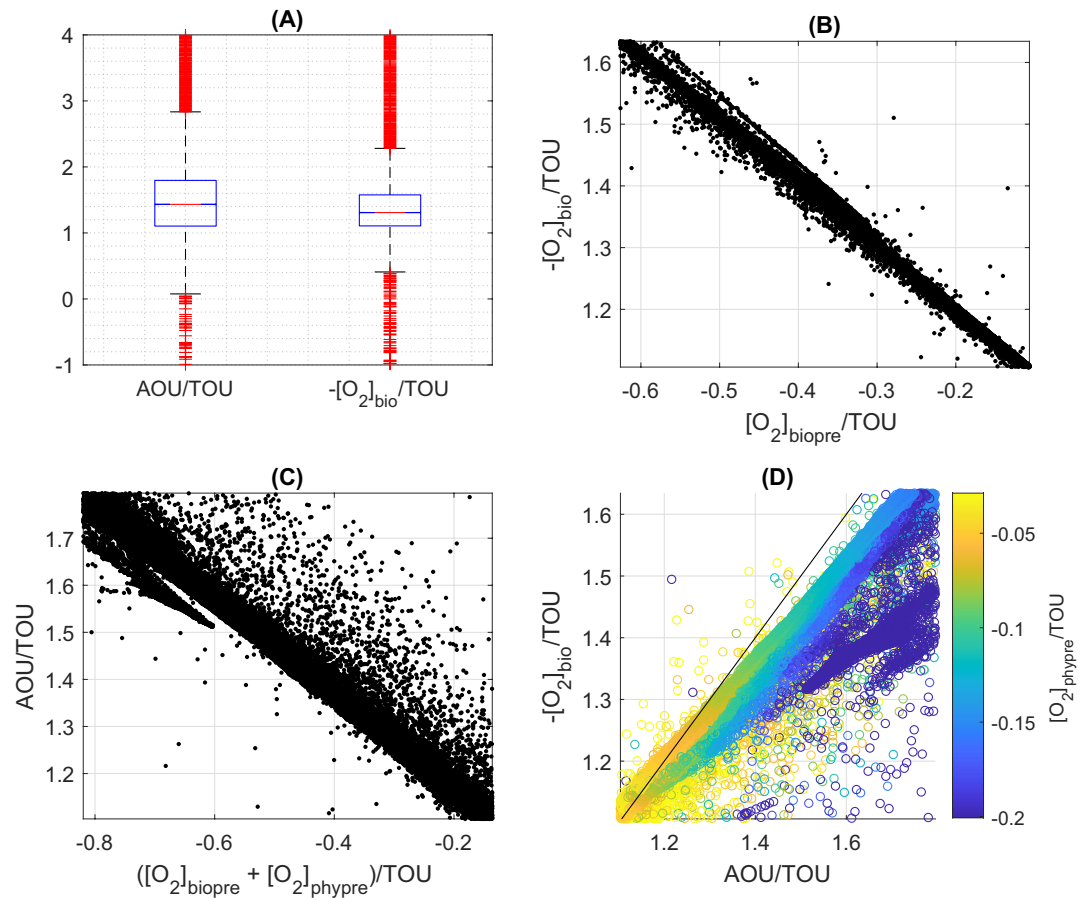
Figure 3. Comparison of modeled apparent oxygen utilization (AOU) with O_2/Ar-derived $[O_2]_{bio}$ in predicting true oxygen utilization (TOU). (a) Box and whisker plot of AOU/TOU and $[O_2]_{bio}$/TOU. The central line in the box indicates the median, and the bottom and top edges of the box indicate the 25th and 75th percentiles, respectively. Black whiskers and the red "+" symbol represent extreme points and outliers, respectively. (b) $[O_2]_{bio}$/TOU as a function of $[O_2]_{biopre}$/TOU. (c) Predictive power of AOU as a function of the preformed $[O_2]$. (d) Relative performance of $[O_2]_{bio}$ and AOU as a function of $[O_2]_{phypre}$. The solid black line represents the identity (1:1) line. In (b–d), the abscissa and ordinate axis limits are set at the 25th and 75th percentiles, respectively.

decrease compared with TOU according to $\dfrac{\text{AOU}}{\text{TOU}} = 1 - \left([O_2]_{phypre} + \Delta[O_2]_{phy} + [O_2]_{biopre} \right)/\text{TOU}$. Lastly, from $\left(\dfrac{-[O_2]_{bio}}{\text{TOU}} \right) - \dfrac{\text{AOU}}{\text{TOU}} = \dfrac{\left([O_2]_{phypre} + \Delta[O_2]_{phy} \right)}{\text{TOU}}$, the net improvement in the predictive power of $[O_2]_{bio}$ over AOU is greatest when the contribution of $\left([O_2]_{phypre} + \Delta[O_2]_{phy} \right)$ to TOU is largest (Figure 3d). For a geospatial context, Figure 4 presents a subset of the data in Figure 3 along a meridional transect in the Atlantic Ocean. The performance of $[O_2]_{bio}$ and AOU and the difference in their performance (Figures 4a, 4c and 4e, respectively) are displayed in relation to the corresponding factors influencing their performance (Figures 4b, 4d, and 4f). Evidently, AOU and $[O_2]_{bio}$ perform best in shallower meso and bathypelagic extrapolar waters, where the contribution of $[O_2]_{biopre}$ and $\left([O_2]_{phypre} + [O_2]_{biopre} \right)$ to TOU, respectively, is lowest. Both tracers perform poorly in Antarctic Bottom Waters (AABW) and North Atlantic Deep Water (NADW). However, $[O_2]_{bio}$ performs significantly better than AOU because of the large $[O_2]_{phypre}$ contribution to TOU in these waters and deeper waters in general. Based on these model simulations, this is where the added value of $[O_2]_{bio}$ over AOU is greatest.
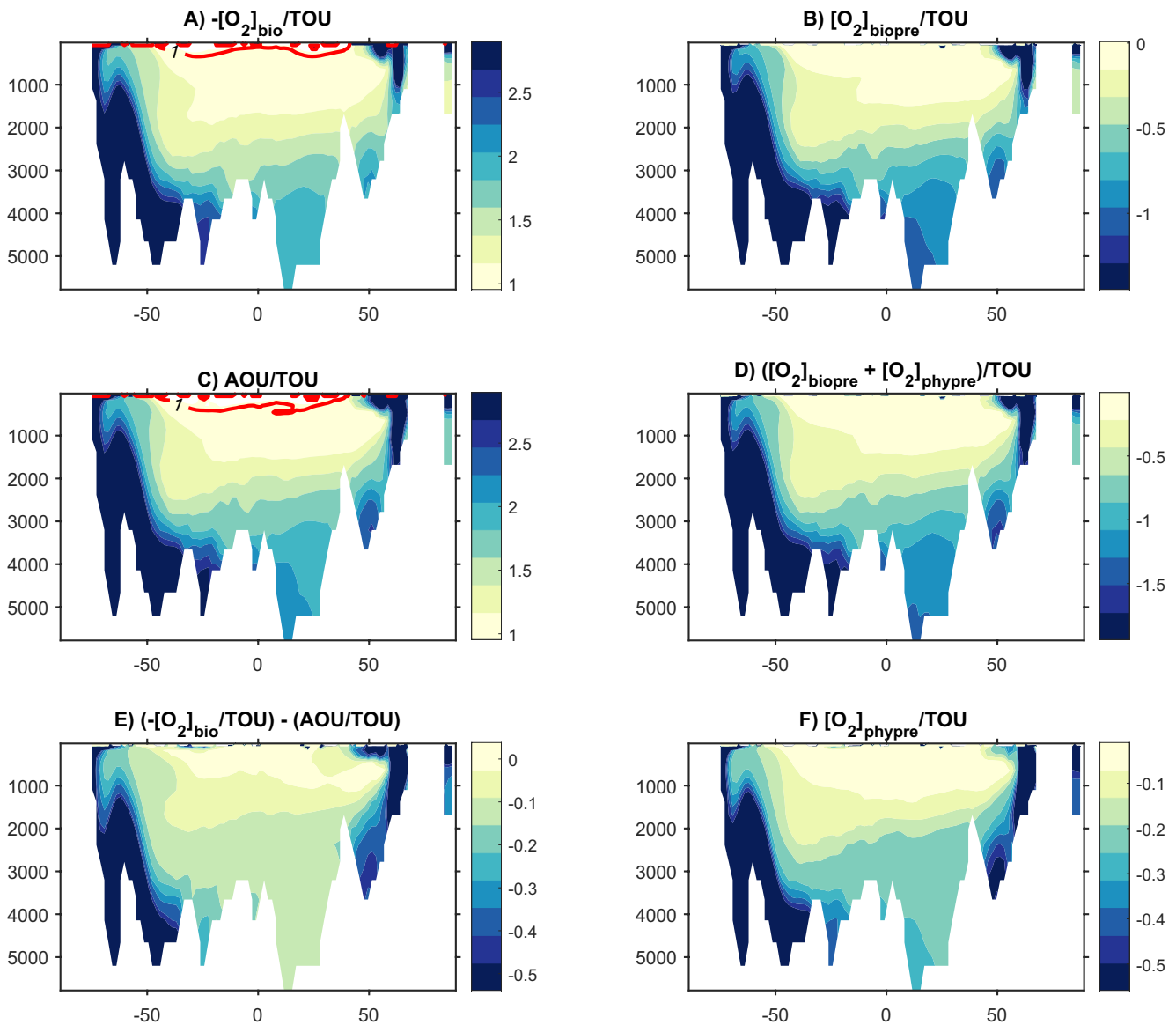
Figure 4. Latitudinal variations at 30°W (Atlantic Ocean) in the relative performance of modeled (a) O_2/Ar-derived $[O_2]_{bio}$ and (c) apparent oxygen utilization (AOU) in predicting True Oxygen Utilization (TOU) as a function of (b) $[O_2]_{biopre}$/TOU and (d) $\left([O_2]_{biopre} + [O_2]_{phypre}\right)$/TOU. Red lines in panels (a and c) represent isopleths of no biases in each tracers estimate of TOU, that is, $-[O_2]_{bio}$/TOU = 1 and AOU/TOU = 1, respectively. (e) The relative improvement of $[O_2]_{bio}$ compared to AOU is a function of (f) $[O_2]_{phypre}$/TOU. Abscissa and ordinate reflect latitude and depth, respectively. Extreme values are not visible because the color map limits are set at the 10th and 90th percentiles for each subplot, except for (a) that is set to the same limits as (c) for comparison.

5. Implications for Remineralization Ratios, Preformed and Regenerated Phosphate, and Gas Exchange at the Sites of Deepwater Formation

The aforementioned discussion has implications for estimates of remineralization ratios and preformed and regenerated properties, which have been used to quantify the efficiency of the biological pump (e.g., Ito & Follows, 2013). Using the same data-constrained physical–biogeochemical model as Cliff et al. (2021), Khatiwala et al. (2019) found that the AOU overestimated the inventory of remineralized carbon by almost 50%. One direct consequence of the work presented here is that $[O_2]_{bio}$ can reduce this bias. While the reduction is found to be modest, it could be significant in some regions and furthermore, for the reasons described above, should be regarded as a lower bound on the potential improvement that can be achieved. Whereas O_2 is influenced by gas exchange at the sites of deepwater formation, phosphate is conservative with respect
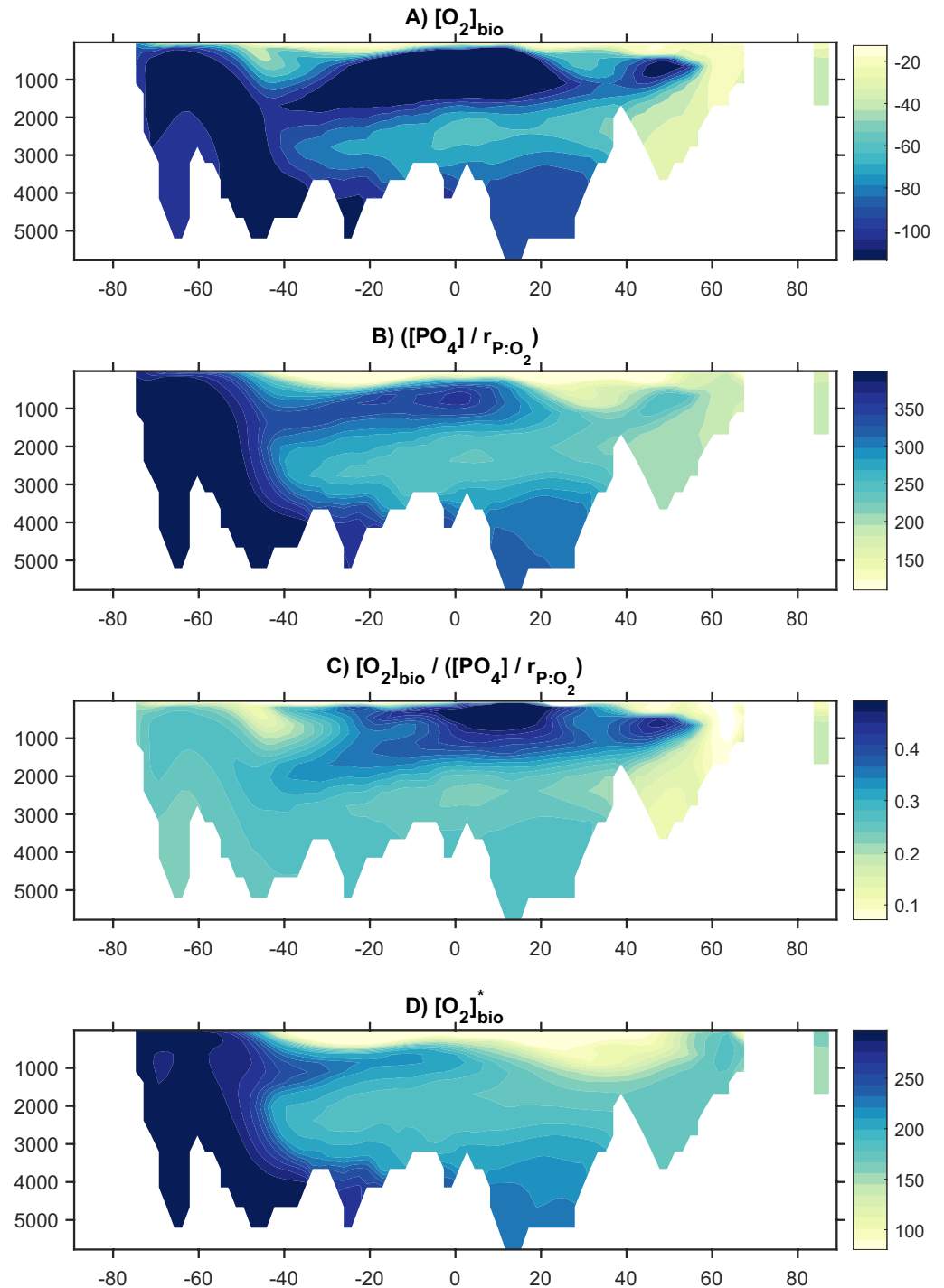
Figure 5. Latitudinal variations at 30°W (Atlantic Ocean) in depth profiles modeled (a) O_2/Ar-derived $[O_2]_{bio}$, (b) $[PO_4]/r_{P:O2}$ (phosphate in O_2 equivalents), (c) their relative magnitude $\left([O_2]_{bio}/\left([PO_4]/r_{P:O2}\right)\right)$, and contribution to (d) $[O_2]_{bio}^*$. Concentrations are in mmol m^{-3}. Abscissa and ordinate reflect latitude and depth, respectively. Extreme values are not visible because the color map limits are set at the 10th and 90th percentiles for each subplot.

to gas exchange. Operationally, the $[O_2]_{biopre} = [O_2]_{bio} - \Delta[O_2]_{Rem}$ tracer is analogous to the preformed phosphate tracer (Broecker, 1974; Broecker et al., 1985):

$$\left[PO_4\right]_{pre} = \left[PO_4\right] - \Delta\left[PO_4\right]_{rem} \tag{8}$$

Traditionally, $[PO_4]_{pre}$ has been estimated as follows under the assumption that $\left([O_2]_{phy} + [O_2]_{biopre}\right) = 0$:

$$\left[PO_4\right]_{pre} = \left[PO_4\right] + r_{P:O2}\,AOU \tag{9}$$

where $r_{P:O2}$ is the $PO_4{:}O_2$ remineralization ratio and is generally assumed constant at approximately -170 ± 10 (Anderson & Sarmiento, 1994). Duteil et al. (2013) showed that the assumption of atmospheric equilibrium at the sites of deepwater formation leads to a substantial underestimation of the fraction of preformed phosphate at depth. The effect is compounded by uncertainties in the elemental stoichiometry during remineralization when estimating the proportion of regenerated and preformed nutrients from the oxygen concentration. The $[O_2]_{bio}$ tracer can reduce the uncertainties both in the remineralization ratios (e.g., $r_{P:O2}$ in Equation 9) and oxygen utilization at depth (AOU in Equation 9). In the regions where physical processes impact the total oxygen concentration (e.g., thermocline waters), $[O_2]_{bio}$ could prove to be valuable for studying Redfieldian ratios such as the respiratory quotients and remineralization ratios. Similarly, for water masses where $r_{P:O2}\left([O_2]_{phypre} + \Delta[O_2]_{phy}\right)/[PO_4]_{pre}$ is largest, replacing AOU in Equation 9 with $-[O_2]_{bio}$ from Equation 6 (estimated with O_2/Ar) will improve the estimates of $[PO_4]_{pre}$.

In some regions, the preformed O_2 anomaly can be of the same order of magnitude as the preformed phosphate concentration. O_2 anomalies in regions of deepwater formation such as the Weddell Sea and Ross Sea can be as high as 50–100 μM (Duteil et al., 2013; Ito et al., 2004), corresponding to up to $\sim 0.6\ \mu M$ phosphate equivalents, well within the range of observed preformed phosphate concentrations (Duteil et al., 2012). In these regions, the preformed phosphate as calculated in Equation 9 potentially encapsulates important information about the extent of decoupling between these two properties associated with gas exchange at the sites of deepwater formation. In order to illustrate this dichotomy, we define $[O_2]_{bio}^*$ as:

$$\left[O_2\right]_{bio}^* = \left[O_2\right]_{bio} - \frac{\left[PO_4\right]}{r_{P:O2}} \tag{10}$$

$[O_2]_{bio}^*$ is a property that can be readily estimated in the ocean interior with the dissolved O_2/Ar ratio being a proxy for the first term on the right-hand side (and could help with constraints on $r_{P:O2}$ as discussed above). Conceptually, the $[O_2]_{bio}^*$ term is akin to the O_2^* defined in Gruber et al. (2001) with the important distinction that the first-term on the right-hand side is not the total $[O_2]$ but $[O_2]_{bio}$. In contrast to $[O_2]_{bio}^*$, $[O_2]$ encompasses the effect of temperature and salinity on the solubility of O_2. It is straightforward to show that the relation between synthetic tracers $[O_2]_{bio}^*$ and $[PO_4]_{pre}$ can also be written as:

$$\left[O_2\right]_{bio}^* = \left[O_2\right]_{biopre} - \frac{\left[PO_4\right]_{pre}}{r_{P:O2}} \tag{11}$$

Assuming a constant $r_{P:O2}$ stoichiometric ratio, $[O_2]_{bio}^*$ is therefore conservative with respect to photosynthesis, respiration (and remineralization), and abiotic processes in the ocean interior. The magnitude of $[O_2]_{bio}^*$ should reflect the preformed phosphate concentration ($[PO_4]_{pre}$) and factors influencing the removal of $[O_2]_{bio}$ through air-sea gas exchange (e.g., including wind speed, mixed-layer depth, temperature, and the residence time of water masses at the ocean surface but excluding atmospheric pressure changes). In regions where allochthonous physical phosphate supply (e.g., riverine input) is negligible such as the open ocean, changes in $[O_2]_{bio}^*$ mainly reflect air-sea gas exchange. Bubbles do not impart a significant change in $[O_2]_{biopre}$ (or the dissolved O_2/Ar saturation) but facilitate its equilibration by enhancing the rate of exchange with the atmosphere. When gas exchange at the surface is impaired (e.g., ice cover), the biological O_2 and phosphate signals stay coupled, leading to no change in $[O_2]_{bio}^*$. Conversely, in regions where rapid gas exchange occurs, $[O_2]_{bio}^*$ can increase or decrease. A positive (negative) $[O_2]_{bio}$ associated with a net autotrophic (heterotrophic) system with rapid gas exchange will tend to decrease (increase) $[O_2]_{bio}^*$. $[O_2]_{bio}^*$ is expected to generally increase at the sites of deepwater formation during the winter, decoupling $[O_2]_{biopre}$ from $[PO_4]_{pre}$ through reoxygenation of the ocean surface. The loss of negative $[O_2]_{bio}$ relative to $[PO_4]$ (i.e., increase in $[O_2]_{bio}^*$) due to gas exchange in preformed waters can lead to O_2/Ar supersaturation (from photosynthesis) in upwelled waters reaching the surface even in the absence of gas exchange. This may explain the O_2/Ar supersaturation observed in some ice-covered regions (Eveleth et al., 2014; Ulfsbo et al., 2014).

Our model results show that $[O_2]^*_{bio}$ is particularly positive in AABW, driven primarily by high $[PO_4]_{pre}$ but with a nonnegligible contribution from $[O_2]_{bio}$. Efficient gas exchange and reoxygenation further decouple $[O_2]_{biopre}$ and $[PO_4]_{pre}$ at the ventilation site (Figure 5), consistent with the important role Weddell and Ross Seas coastal (latent heat) polynyas play in the AABW formation (Bromwich & Kurtz, 1984; Cheon et al., 2015; Ohshima et al., 2013).

6. Conclusions

We have shown that the biological oxygen concentration ($[O_2]_{bio}$) at depth can be estimated using the elemental ratio of oxygen and argon (O_2/Ar). This composite geochemical tracer improves on observation-based estimates of biological oxygen utilization in the ocean interior by removing the impact of physical processes on the oxygen signal. Based on our numerical simulations mimicking an Ocean Observing System, the largest improvements compared with traditional AOU estimates are seen in Antarctic Bottom Water and North Atlantic Deep Water. While more work is needed, our results indicate that strategic measurements of O_2/Ar in the ocean interior could improve true oxygen utilization (TOU) estimates. More broadly, our study demonstrates the value in using composite gas ratios such as O_2/Ar, alone or in combination with other tracers, to deconvolve the complex array of physical and biogeochemical processes influencing gases and nutrients in the ocean interior, and ultimately the feedbacks between climate and the strength of the biological carbon pump.

Data Availability Statement

Computing resources were provided by the University of Oxford Advanced Research Computing (ARC) facility (http://dx.doi.org/10.5281/zenodo.22558). Model codes and simulation products are available from https://doi.org/10.5281/zenodo.1246300 and https://doi.org/10.5281/zenodo.4455661, respectively.

References

Anderson, L. A., & Sarmiento, J. L. (1994). Redfield ratios of remineralization determined by nutrient data-analysis. *Global Biogeochemical Cycles*, 8(1), 65–80. https://doi.org/10.1029/93gb03318

Atamanchuk, D., Koelling, J., Send, U., & Wallace, D. W. R. (2020). Rapid transfer of oxygen to the deep ocean mediated by bubbles. *Nature Geoscience*, 13(3), 232. https://doi.org/10.1038/s41561-020-0532-2

Broecker, W. S. (1974). "NO" a conservative water-mass tracer. *Earth and Planetary Science Letters*, 23(1), 100–107. https://doi.org/10.1016/0012-821x(74)90036-3

Broecker, W. S., Blanton, S., Smethie, W. M., & Ostlund, G. (1991). Radiocarbon decay and oxygen utilization in the Deep Atlantic Ocean. *Global Biogeochemical Cycles*, 5(1), 87–117. https://doi.org/10.1029/90GB02279

Broecker, W. S., Takahashi, T., & Takahashi, T. (1985). Sources and flow patterns of deep-ocean waters as deduced from potential temperature, salinity, and initial phosphate concentration. *Journal of Geophysical Research*, 90, 6925–6939. https://doi.org/10.1029/jc090ic04p06925

Bromwich, D. H., & Kurtz, D. D. (1984). Katabatic wind forcing of the Terra-Nova Bay Polynya. *Journal of Geophysical Research-Oceans*, 89(3), 3561–3572. https://doi.org/10.1029/jc089ic03p03561

Cassar, N., Barnett, B. A., Bender, M. L., Kaiser, J., Hamme, R. C., & Tilbrook, B. (2009). Continuous high-frequency dissolved O_2/Ar measurements by equilibrator inlet mass spectrometry. *Analytical Chemistry*, 81(5), 1855–1864. https://doi.org/10.1021/ac802300u

Cassar, N., DiFiore, P. J., Barnett, B. A., Bender, M. L., Bowie, A. R., Tilbrook, B., et al. (2011). The influence of iron and light on net community production in the Subantarctic and Polar Frontal Zones. *Biogeosciences*, 8(2), 227–237. https://doi.org/10.5194/bg-8-227-2011

Cheon, W. G., Lee, S. K., Gordon, A. L., Liu, Y., Cho, C. B., & Park, J. J. (2015). Replicating the 1970s' Weddell Polynya using a coupled ocean-sea ice model with reanalysis surface flux fields. *Geophysical Research Letters*, 42(13), 5411–5418. https://doi.org/10.1002/2015gl064364

Cliff, E., Khatiwala, S., & Schmittner, A. (2021). Glacial deep ocean deoxygenation driven by biologically mediated air–sea disequilibrium. *Nature Geoscience*, 14(1), 43–50. https://doi.org/10.1038/s41561-020-00667-z

Craig, H., & Hayward, T. (1987). Oxygen supersaturation in the ocean - Biological versus physical contributions. *Science*, 235(4785), 199–202. https://doi.org/10.1126/science.235.4785.199

Deutsch, C., Gruber, N., Key, R. M., Sarmiento, J. L., & Ganachaud, A. (2001). Denitrification and N_2 fixation in the Pacific Ocean. *Global Biogeochemical Cycles*, 15(2), 483–506. https://doi.org/10.1029/2000gb001291

DeVries, T., & Primeau, F. (2011). Dynamically and observationally constrained estimates of water-mass distributions and ages in the global ocean. *Journal of Physical Oceanography*, 41(12), 2381–2401. https://doi.org/10.1175/jpo-d-10-05011.1

Duteil, O., Koeve, W., Oschlies, A., Aumont, O., Bianchi, D., Bopp, L., et al. (2012). Preformed and regenerated phosphate in ocean general circulation models: Can right total concentrations be wrong? *Biogeosciences*, 9(5), 1797–1807. https://doi.org/10.5194/bg-9-1797-2012

Duteil, O., Koeve, W., Oschlies, A., Bianchi, D., Galbraith, E., Kriest, I., & Matear, R. (2013). A novel estimate of ocean oxygen utilisation points to a reduced rate of respiration in the ocean interior. *Biogeosciences*, 10(11), 7723–7738. https://doi.org/10.5194/bg-10-7723-2013

Emerson, S., Ito, T., & Hamme, R. C. (2012). Argon supersaturation indicates low decadal-scale vertical mixing in the ocean thermocline. *Geophysical Research Letters*, 39. https://doi.org/10.1029/2012gl053054

Enns, T., Scholand, P., & Bradstre (Eds.), (1965). Effect of hydrostatic pressure on gases dissolved in water. *Journal of Physical Chemistry*. *69*, (pp. 389–91).

Eveleth, R., Cassar, N., Doney, S. C., Munro, D. R., & Sweeney, C. (2017). Biological and physical controls on O_2/Ar, Ar and pCO_2 variability at the Western Antarctic Peninsula and in the Drake Passage. *Deep Sea Research Part II: Topical Studies in Oceanography*, *139*, 77–88. https://doi.org/10.1016/j.dsr2.2016.05.002

Eveleth, R., Timmermans, M. L., & Cassar, N. (2014). Physical and biological controls on oxygen saturation variability in the upper Arctic Ocean. *Journal of Geophysical Research-Oceans*, *119*(11), 7420–7432. https://doi.org/10.1002/2014jc009816

Garcia, H. E., & Gordon, L. I. (1992). Oxygen solubility in seawater - Better fitting equations. *Limnology & Oceanography*, *37*(6), 1307–1312. https://doi.org/10.4319/lo.1992.37.6.1307

Gruber, N., Gloor, M., Fan, S. M., & Sarmiento, J. L. (2001). Air-sea flux of oxygen estimated from bulk data: Implications for the marine and atmospheric oxygen cycles. *Global Biogeochemical Cycles*, *15*(4), 783–803. https://doi.org/10.1029/2000gb001302

Gruber, N., & Sarmiento, J. L. (1997). Global patterns of marine nitrogen fixation and denitrification. *Global Biogeochemical Cycles*, *11*(2), 235–266. https://doi.org/10.1029/97gb00077

Gueguen, C., & Tortell, P. D. (2008). High-resolution measurement of Southern Ocean CO_2 and O_2/Ar by membrane inlet mass spectrometry. *Marine Chemistry*, *108*(3–4), 184–194. https://doi.org/10.1016/j.marchem.2007.11.007

Haine, T. W. N., & Hall, T. M. (2002). A generalized transport theory: Water-mass composition and age. *Journal of Physical Oceanography*, *32*(6), 1932–1946. https://doi.org/10.1175/1520-0485(2002)032.1932:agttwm.2.0.co;2

Hamme, R. C., Cassar, N., Lance, V. P., Vaillancourt, R. D., Bender, M. L., Strutton, P. G., et al. (2012). Dissolved O_2/Ar and other methods reveal rapid changes in productivity during a Lagrangian experiment in the Southern Ocean. *Journal of Geophysical Research*, *117*. https://doi.org/10.1029/2011JC007046

Hamme, R. C., & Emerson, S. R. (2002). Mechanisms controlling the global oceanic distribution of the inert gases argon, nitrogen and neon. *Geophysical Research Letters*, *29*(23). https://doi.org/10.1029/2002gl015273

Hamme, R. C., & Emerson, S. R. (2004). The solubility of neon, nitrogen and argon in distilled water and seawater. *Deep Sea Research Part I: Oceanographic Research Papers*, *51*(11), 1517–1528. https://doi.org/10.1016/j.dsr.2004.06.009

Hamme, R. C., Nicholson, D. P., Jenkins, W. J., & Emerson, S. R. (2019). Using noble gases to assess the ocean's carbon pumps. *Annual Review of Marine Science*, *11*(1), 75–103. https://doi.org/10.1146/annurev-marine-121916-063604

Hamme, R. C., & Severinghaus, J. P. (2007). Trace gas disequilibria during deep-water formation. *Deep Sea Research Part I: Oceanographic Research Papers*, *54*(6), 939–950. https://doi.org/10.1016/j.dsr.2007.03.008

Hellmer, H. H., Jacobs, S. S., & Jenkins, A. (1985). Oceanic Erosion of a Floating Antarctic Glacier in the Amundsen Sea. *Ocean, ice, and atmosphere: Interactions at the antarctic continental margin* (pp. 83–99).

Henning, C. C., Archer, D., & Fung, I. (2006). Argon as a tracer of cross-isopycnal mixing in the thermocline. *Journal of Physical Oceanography*, *36*(11), 2090–2105. https://doi.org/10.1175/jpo2961.1

Huang, K., Ducklow, H., Vernet, M., Cassar, N., & Bender, M. L. (2012). Export production and its regulating factors in the West Antarctica Peninsula region of the Southern Ocean. *Global Biogeochemical Cycles*, *26*. https://doi.org/10.1029/2010gb004028

Ito, T., & Deutsch, C. (2006). Understanding the saturation state of argon in the thermocline: The role of air-sea gas exchange and diapycnal mixing. *Global Biogeochemical Cycles*, *20*(3). https://doi.org/10.1029/2005gb002655

Ito, T., Deutsch, C., Emerson, S., & Hamme, R. C. (2007). Impact of diapycnal mixing on the saturation state of argon in the subtropical North Pacific. *Geophysical Research Letters*, *34*(9). https://doi.org/10.1029/2006gl029209

Ito, T., & Follows, M. J. (2013). Air-sea disequilibrium of carbon dioxide enhances the biological carbon sequestration in the Southern Ocean. *Global Biogeochemical Cycles*, *27*(4), 1129–1138. https://doi.org/10.1002/2013gb004682

Ito, T., Follows, M. J., & Boyle, E. A. (2004). Is AOU a good measure of respiration in the oceans? *Geophysical Research Letters*, *31*(17). https://doi.org/10.1029/2004gl020900

Jenkins, A. (1999). The impact of melting ice on ocean waters. *Journal of Physical Oceanography*, *29*(9), 2370–2381. https://doi.org/10.1175/1520-0485(1999)029.2370:tiomio.2.0.co;2

Khatiwala, S. (2007). A computational framework for simulation of biogeochemical tracers in the ocean. *Global Biogeochemical Cycles*, *21*(3). https://doi.org/10.1029/2007gb002923

Khatiwala, S. (2018). *Transport Matrix Method software for ocean biogeochemical simulations*. Publication. https://doi.org/10.5281/zenodo

Khatiwala, S., Primeau, F., & Holzer, M. (2012). Ventilation of the deep ocean constrained with tracer observations and implications for radiocarbon estimates of ideal mean age. *Earth and Planetary Science Letters*, *325–326*, 116–125. https://doi.org/10.1016/j.epsl.2012.01.038

Khatiwala, S., Schmittner, A., & Muglia, J. (2019). Air-sea disequilibrium enhances ocean carbon storage during glacial periods. *Science Advances*, *5*(6). https://doi.org/10.1126/sciadv.aaw4981

Khatiwala, S., Visbeck, M., & Cane, M. A. (2005). Accelerated simulation of passive tracers in ocean circulation models. *Ocean Modelling*, *9*(1), 51–69. https://doi.org/10.1016/j.ocemod.2004.04.002

Klots, C. E. (1961). Effect of hydrostatic pressure upon the solubility of gases. *Limnology & Oceanography*, *6*(3), 365–366. https://doi.org/10.4319/lo.1961.6.3.0365

Koeve, W., Kähler, P., & Oschlies, A. (2020). Does export production measure transient changes of the biological carbon pump's feedback to the atmosphere under global warming? *Geophysical Research Letters*, e2020GL089928. https://doi.org/10.1029/2020GL089928

Kortzinger, A., Schimanski, J., Send, U., & Wallace, D. (2004). The ocean takes a deep breath. *Science*, *306*(5700), 1337–1337. https://doi.org/10.1126/science.1102557

Long, M. C., Dunbar, R. B., Tortell, P. D., Smith, W. O., Mucciarone, D. A., & DiTullio, G. R. (2011). Vertical structure, seasonal drawdown, and net community production in the Ross Sea, Antarctica. *Journal of Geophysical Research*, *116*. https://doi.org/10.1029/2009jc005954

Martinerie, P., Raynaud, D., Etheridge, D. M., Barnola, J. M., & Mazaudier, D. (1992). Physical and climatic parameters which influence the air content in polar ice. *Earth and Planetary Science Letters*, *112*(1–4), 1–13. https://doi.org/10.1016/0012-821x(92)90002-d

Nicholson, D. P., Khatiwala, S., & Heimbach, P. (2016). Noble gas tracers of ventilation during deep-water formation in the Weddell Sea. *IOP Conference Series: Earth and Environmental Science*, *35*, 012019. https://doi.org/10.1088/1755-1315/35/1/012019

Ohshima, K. I., Fukamachi, Y., Williams, G. D., Nihashi, S., Roquet, F., Kitade, Y., et al. (2013). Antarctic bottomwater production by intense sea-ice formation in the Cape Darnley polynya. *Nature Geoscience*, *6*(3), 235–240. https://doi.org/10.1038/ngeo1738

Palevsky, H. I., Ribalet, F., Swalwell, J. E., Cosca, C. E., Cokelet, E. D., Feely, R. A., et al. (2013). The influence of net community production and phytoplankton community structure on CO_2 uptake in the Gulf of Alaska. *Global Biogeochemical Cycles*, *27*(3), 664–676. https://doi.org/10.1002/gbc.20058

Primeau, F. (2005). Characterizing transport between the surface mixed layer and the ocean interior with a forward and adjoint global ocean transport model. *Journal of Physical Oceanography*, *35*(4), 545–564. https://doi.org/10.1175/jpo2699.1

Redfield, A. C., Ketchum, B. H., & Richards, F. A. (1963). The influence of organisms on the composition of seawater. In M. N. Hill (Ed.), The sea (Vol. 2). Interscience.

Reuer, M. K., Barnett, B. A., Bender, M. L., Falkowski, P. G., & Hendricks, M. B. (2007). New estimates of Southern Ocean biological production rates from O_2/Ar Ratios and the triple isotope composition of O_2. *Deep-Sea Research I*, *54*, 951–974. https://doi.org/10.1016/j.dsr.2007.02.007

Shiller, A. M. (1981). Calculating the Oceanic CO_2 Increase - A Need for Caution. *Journal of Geophysical Research-Oceans and Atmospheres*, *86*, 1083–1088. https://doi.org/10.1029/jc086ic11p11083

Spitzer, W. S., & Jenkins, W. J. (1989). Rates of vertical mixing, gas-exchange and new production - Estimates from seasonal gas cycles in the upper ocean near Bermuda. *Journal of Marine Research*, *47*(1), 169–196. https://doi.org/10.1357/002224089785076370

Sun, D. X., Ito, T., & Bracco, A. (2017). Oceanic uptake of oxygen during deep convection events through diffusive and bubble-mediated gas exchange. *Global Biogeochemical Cycles*, *31*(10), 1579–1591. https://doi.org/10.1002/2017gb005716

Top, Z., Martin, S., & Becker, P. (1985). On the dissolved surface oxygen supersaturation in the Arctic. *Geophysical Research Letters*, *12*(12), 821–823. https://doi.org/10.1029/gl012i012p00821

Top, Z., Martin, S., & Becker, P. (1988). A laboratory study of dissolved noble-gas anomaly due to ice formation. *Geophysical Research Letters*, *15*(8), 796–799. https://doi.org/10.1029/gl015i008p00796

Ulfsbo, A., Cassar, N., Korhonen, M., van Heuven, S., Hoppema, M., Kattner, G., & Anderson, L. G. (2014). Late summernet community production in the central Arctic Ocean using multiple approaches. *Global Biogeochemical Cycles*, *28*(10), 1129–1148. https://doi.org/10.1002/2014gb004833

Wise, D. L., & Houghton, G. (1966). Diffusion coefficients of 10 slightly soluble gases in water at 10–60°C. *Chemical Engineering Science*, *21*(11), 999–1010. https://doi.org/10.1016/0009-2509(66)85096-0

Wolf, M. K., Hamme, R. C., Gilbert, D., Yashayaev, I., & Thierry, V. (2018). Oxygen saturation surrounding deep water formation events in the labrador sea from Argo-O_2 data. *Global Biogeochemical Cycles*, *32*(4), 635–653. https://doi.org/10.1002/2017gb005829

References From the Supporting Information

Garcia, H. E., Locarnini, R. A., Boyer, T. P., Antonov, J. I., Zweng, M. M., Baranova, O. K., & Johnson, D. R. (2010). *World ocean atlas 2009*. In Nutrients (Phosphate, Nitrate, Silicate) (Vol. 4).

Jenkins, W. J., Lott, D. E., & Cahill, K. L. (2019). A determination of atmospheric helium, neon, argon, krypton, and xenon solubility concentrations in water and seawater. *Marine Chemistry*, *211*, 94–107. https://doi.org/10.1016/j.marchem.2019.03.007

Muglia, J., & Schmittner, A. (2015). Glacial Atlantic overturning increased by wind stress in climate models. *Geophysical Research Letters*, *42*(22), 9862–9868. https://doi.org/10.1002/2015gl064583

Muglia, J., Skinner, L. C., & Schmittner, A. (2018). Weak overturning circulation and high Southern Ocean nutrient utilization maximized glacial ocean carbon. *Earth and Planetary Science Letters*, *496*, 47–56. https://doi.org/10.1016/j.epsl.2018.05.038

Wanninkhof, R. (1992). Relationship between wind-speed and gas-exchange over the ocean. *Journal of Geophysical Research*, *97*(C5), 7373–7382. https://doi.org/10.1029/92jc00188

Weaver, A. J., Eby, M., Wiebe, E. C., Bitz, C. M., Duffy, P. B., Ewen, T. L., et al. (2001). The UVic earth system climate model: Model description, climatology, and applications to past, present and future climates. *Atmosphere*, *39*(4), 361–428. https://doi.org/10.1080/07055900.2001.9649686